Thermochimica Acta 519 (2011) 96–102

Contents lists available at ScienceDirect

Thermochimica Acta

journal homepage: www.elsevier.com/locate/tca

Simultaneous measurements of thermal conductivity, thermal diffusivity and specific heat by nuclear magnetic resonance imaging

David H. Gultekin[a,b,c,*], John C. Gore[d,e,f,g,h]

[a] Engineering and Applied Science, Yale University, New Haven, CT 06520, USA
[b] Department of Medical Physics, Memorial Sloan-Kettering Cancer Center, New York, NY 10065, USA
[c] Department of Radiology, Memorial Sloan-Kettering Cancer Center, New York, NY 10065, USA
[d] Department of Biomedical Engineering, Vanderbilt University, Nashville, TN 37232, USA
[e] Department of Radiology and Radiological Sciences, Vanderbilt University, Nashville, TN 37232, USA
[f] Department of Molecular Physiology and Biophysics, Vanderbilt University, Nashville, TN 37232, USA
[g] Department of Physics and Astronomy, Vanderbilt University, Nashville, TN 37232, USA
[h] Institute of Imaging Science, Vanderbilt University, Nashville, TN 37232, USA

ARTICLE INFO

Article history:
Received 24 January 2011
Received in revised form 23 February 2011
Accepted 26 February 2011
Available online 21 March 2011

Keywords:
Thermal conductivity
Thermal diffusivity
Specific heat
NMR calorimetry
Thermometry

ABSTRACT

The feasibility of measuring the thermal conductivity (κ), thermal diffusivity (α) and specific heat (c_p) of an aqueous gel noninvasively by nuclear magnetic resonance (NMR) imaging is presented. NMR images acquired with high spatial and temporal resolutions provide the means for a direct evaluation of Fourier's heat conduction relation and the simultaneous measurement of κ, α and c_p in a single experiment. An aqueous gel is heated by a diode laser absorbed in a silicon wafer providing a planar constant heat flux boundary condition, and the subsequent spatial and temporal variations of temperature in the gel are measured by changes in the water proton resonance frequency and consequent nuclear spin phase shifts in gradient echo images. The evaluation of the spatial and temporal variations of temperature yields the diffusion length and thermal diffusivity, the ratio of nuclear thermal coefficient to the thermal conductivity; and the temporal variation of the spatially averaged nuclear spin phase shift yields the ratio of heat capacity to the nuclear thermal coefficient. The temporal trajectory of the diffusion length (λ) is found to be independent of heat flux (f_0). Furthermore, a direct evaluation of nuclear spin phase shift gradients corresponding to long times and short distances from the heat flux boundary directly yields the ratio of nuclear thermal coefficient to the thermal conductivity per Fourier's heat conduction relation.

1. Introduction

The measurement of thermal properties of hydrated substances is important in many fields including materials science, food science, biology and medicine. Measurement techniques in thermal science have focused mainly on calorimetry [1,2] and thermal transport properties [3] which have a wide range of applications. There have been many advances and variations in the methods used for the measurement of specific heat, thermal diffusivity and thermal conductivity depending on the experimental and thermodynamic conditions. The specific heat is mainly measured by differential scanning calorimetry (DSC) [4] and modulated temperature differential scanning calorimetry (MTDSC) [5,6], the thermal diffusivity is often measured by a thermal pulse method [7] and the thermal conductivity is measured by a transient hot wire (THW) technique [8,9] or a transient hot disk or transient plane source (TPS) instrument [10]. However, all of these methods rely on the measurement of temperature at the contact surface or at a finite distance, and they do not detect the temperature gradients through the volume of a substance. Moreover, in substances with low thermal conductivity, the diffusion length for heat is small and temperature gradients form over a short distance, which leads to further limitations for invasive measurements of the temperature gradients. A non-invasive measurement of thermal properties using nuclear magnetic resonance (NMR) imaging may thus find novel and practical applications. NMR images can be acquired from proton-rich materials with high spatial and temporal resolutions and thus can provide the means for the simultaneous measurement of thermal conductivity (κ), thermal diffusivity (α) and specific heat (c_p) in a single experiment using Fourier's heat conduction relation. NMR can directly map thermal gradients in aqueous media

* Corresponding author at: Department of Medical Physics, Memorial Sloan-Kettering Cancer Center, 1275 York Avenue, New York, NY 10065, USA.
Tel.: +1 212 639 7359.
E-mail addresses: david.gultekin@aya.yale.edu, gultekid@mskcc.org (D.H. Gultekin).

0040-6031/$ – see front matter © 2011 Elsevier B.V. All rights reserved.
doi:10.1016/j.tca.2011.02.041

and the temporal evolution of temperature gradients can be measured noninvasively accurately using Fourier's relation. We have previously demonstrated NMR methods for the measurements of thermal conductivity [11,12], thermal diffusivity [13–15] and specific heat [16,17] in liquids. Here, we demonstrate an NMR method to measure all three simultaneously in an aqueous gel using a diode laser and a silicon wafer as a planar heat source.

2. Theory

When a thermal flux is maintained at the surface of a stationary substance, a temperature gradient is formed in the direction perpendicular to the plane of thermal flux. The thermal flux is proportional to the temperature gradient through the thermal conductivity by Fourier's relation as

$$f = -\kappa \nabla T \tag{1}$$

where f is the thermal (heat) flux, κ is the thermal conductivity and ∇T is the temperature gradient [18,19]. The heat increases the temperature of the material and in water this changes the effective nuclear shielding of the hydrogen nuclei (protons) [20,21] causing a shift in the proton resonance frequency.

The spatial variation of nuclear shielding (σ) can be related to the spatial variation of temperature (T) as

$$\frac{\partial \sigma}{\partial z} = \frac{\partial \sigma}{\partial T}\frac{\partial T}{\partial z} \tag{2}$$

Substituting Eq. (2) in Eq. (1), the heat flux in terms of nuclear shielding in one dimension becomes,

$$f = -\frac{\kappa}{\sigma_T}\frac{\partial \sigma}{\partial z} \tag{3}$$

where $\sigma_T = \partial\sigma/\partial T$ is the nuclear thermal coefficient for shielding which can be measured using high resolution NMR techniques and which varies for different substances depending on the atomic and molecular configuration [21].

In the medium that is heated, the heat flux varies spatially and temporally, but its variation in one dimension ($z > 0$, $t > 0$) satisfies the diffusion equation [18].

$$\frac{\partial f}{\partial t} = \alpha \frac{\partial^2 f}{\partial z^2} \tag{4}$$

where $\alpha = \kappa/\rho c_p$ is the thermal diffusion coefficient, κ is the thermal conductivity, ρ is density and c_p is the specific heat of the substance. For a semi-infinite medium with a constant flux boundary condition ($f = f_0$, $z = 0$) the solution in one dimension is

$$f(z,t) = f_0 erfc\left(\frac{z}{2\sqrt{\alpha t}}\right) \tag{5}$$

where *erfc* is the complimentary *error* function.

With NMR, the change in nuclear shielding can be quantified spatially by measuring the spin phase shift that evolves over a known time interval in a gradient echo sequence

$$\phi(T) = \gamma \cdot (1 - \sigma(T)) B_0 \cdot T_E \tag{6}$$

where $\phi(T)$ and $\sigma(T)$ are the nuclear spin phase shift and shielding, respectively, and both are temperature dependent, γ is the gyromagnetic ratio, B_0 is the magnetic field and T_E is the echo time.

The first order derivative of Eq. (6) with respect to space in one direction is

$$\frac{\partial \phi}{\partial z} = -\gamma B_0 T_E \frac{\partial \sigma}{\partial z} \tag{7}$$

and with respect to temperature is

$$\frac{\partial \phi}{\partial T} = -\gamma B_0 T_E \frac{\partial \sigma}{\partial T} \tag{8}$$

Thus, we can write

$$\phi_T = -\gamma \cdot B_0 \cdot T_E \cdot \sigma_T \tag{9}$$

where $\phi_T = \partial\phi/\partial T$ and $\sigma_T = \partial\sigma/\partial T$ are the nuclear thermal coefficients for nuclear spin phase shift and nuclear shielding, respectively [21]. These thermal coefficients depend on the substance and can be determined experimentally by measuring the change in resonant frequency as a function of temperature.

Substituting Eqs. (7) and (8) into Eq. (3), the heat flux becomes

$$f(z,t) = -\frac{\kappa}{\phi_T}\frac{\partial \phi(z,t)}{\partial z} \tag{10}$$

and substituting Eq. (10) into Eq. (5) we find

$$\frac{\partial \phi(z,t)}{\partial z} = -f_0 \frac{\phi_T}{\kappa} erfc\left(\frac{z}{2\sqrt{\alpha t}}\right) \tag{11}$$

the nuclear spin phase shift gradient as a function of space and time. For short distances and long times, the limit of Eq. (11) approaches Fourier's relation as

$$f_0 = -\frac{\kappa}{\phi_T}\left(\frac{\partial \phi(z,t)}{\partial z}\right)_{z\to 0, t\to\infty} \tag{12}$$

where a plot of f_0 vs. $\nabla\phi$ yields a slope equal to $-\kappa/\phi_T$, the ratio of thermal conductivity to the respective nuclear thermal coefficient.

The solution of Eq. (11) in terms of nuclear spin phase shift results in

$$\phi(z,t) = \phi(z,\infty) + f_0 \frac{\phi_T}{\kappa}\left[\frac{2\sqrt{\alpha t}}{\sqrt{\pi}} \exp\left(-\frac{z^2}{4\alpha t}\right) - z \cdot erfc\left(\frac{z}{2\sqrt{\alpha t}}\right)\right] \tag{13}$$

And setting the $\phi(z, \infty) = 0$ using the nuclear spin phase difference we have

$$\phi(z,t) = f_0 \frac{\phi_T}{\kappa}\left[\frac{\lambda}{\sqrt{\pi}} \exp\left(-\frac{z^2}{\lambda^2}\right) - z \cdot erfc\left(\frac{z}{\lambda}\right)\right] \tag{14}$$

where $\lambda = 2\sqrt{\alpha t}$ is the root mean square diffusion length.

Experimental measurements of $\phi(z,t)$ can be numerically fit to Eq. (14) with a high level of precision and both $f_0\phi_T/\kappa$ and λ can be measured experimentally. The nuclear spin phase shift can also be evaluated at very short distances ($z = 0$) from the constant flux boundary when Eq. (14) can be reduced to the following relation.

$$\phi_0 = f_0 \frac{\phi_T}{\kappa}\frac{\lambda}{\sqrt{\pi}} \tag{15}$$

where $\phi_0 = \phi(0,t)$, the nuclear spin phase shift at the surface (ϕ_0), varying with diffusion length (λ) linearly with a constant slope (S_0) as

$$\frac{\partial \phi_0}{\partial \lambda} = f_0 \frac{\phi_T}{\kappa}\frac{1}{\sqrt{\pi}} = S_0 \tag{16}$$

In the case of variable heat flux, the slope (S_0) will vary linearly with heat flux (f_0) as

$$\frac{\partial S_0}{\partial f_0} = \frac{\phi_T}{\kappa}\frac{1}{\sqrt{\pi}} \tag{17}$$

Consequently, a plot of λ vs. $t^{1/2}$ will yield a line with a slope of $2\sqrt{\alpha}$ and a plot of ϕ_0 vs. λ will yield a line with a slope of $f_0\phi_T/\kappa\sqrt{\pi}$ and a plot of S_0 vs. f_0 will yield a line with a slope of $\phi_T/\kappa\sqrt{\pi}$ as shown above.

Over a narrow temperature range, a relation between the spatially averaged thermal energy (Q) and spatially averaged nuclear spin phase shift (ϕ) can be written as

$$\partial Q = \frac{\partial Q}{\partial \phi}\partial\phi = \frac{\partial Q}{\partial T}\frac{\partial T}{\partial \phi}\partial\phi \tag{18}$$

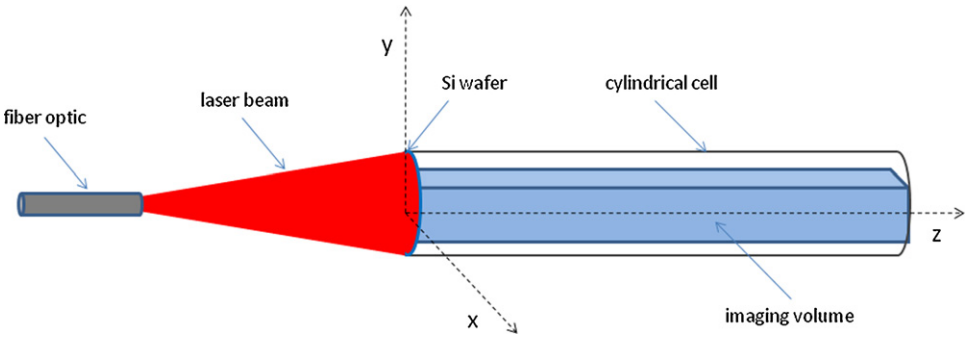

Fig. 1. Schematic diagram of the thermal cell and the experimental setup for 1D heat conduction. The laser energy is absorbed in silicon wafer providing a planar constant flux boundary condition.

Taking the temporal derivatives of both sides and rearranging will yield

$$\dot{Q} = \frac{C_T}{\phi_T}\dot{\phi} \tag{19}$$

where $\dot{Q} = \partial Q/\partial t$ is the thermal power, $C_T = \partial Q/\partial T$ is the heat capacity, $\phi_T = \partial\phi/\partial T$ is the nuclear thermal coefficient for spin phase shift and $\dot{\phi} = \partial\phi/\partial t$ is the rate of nuclear spin phase shift. A first order derivative of $\dot{Q}$ with respect to $\dot{\phi}$ yields

$$\frac{\partial\dot{Q}}{\partial\dot{\phi}} = \frac{C_T}{\phi_T} \tag{20}$$

A plot of $\dot{Q}$ vs. $\dot{\phi}$ will yield a line with a slope of C_T/ϕ_T, the ratio of heat capacity to the respective nuclear thermal coefficient. The heat capacity (C_T) is proportional to specific heat (c_p) through the mass (m) as $C_T = mc_p$ and from this the specific heat (c_p) can be determined experimentally for the substance [17].

3. Experimental methods

As a demonstration of the proposed method, an aqueous gel sample of 3% agarose and water was subjected to heating at the surface by a diode laser in a 2 T magnet and the temporal and spatial variation of the temperature in the gel was measured using the proton resonance frequency [21] and nuclear spin phase shift from the water [22].

A continuous wave (CW) laser beam with a wavelength of 810 nm was used as a thermal source and an electronic grade silicon wafer with an absorptance (A) and a contact surface area (s) was used to absorb and confine the thermal energy into a planar heat source and provide a constant flux boundary condition. The absorptance ($A = 0.16$) was optically measured [23] and the surface area in contact with the gel was measured ($s = 7.854 \times 10^{-5}$ m^2) for the cell. The laser beam was aimed through an optical fiber directly at the silicon wafer in contact with the agarose gel. A schematic diagram of the thermal cell and the experimental setup is given in Fig. 1.

The agarose gel in a cylindrical cell ($D = 10$ mm, $L = 50$ mm) with its axis aligned with the direction of B_0 field (z) was subjected to heating at one end ($z = 0$) using the laser power (P) levels of 0.16, 0.24 and 0.32 W corresponding to heat flux (f_0) levels of 2037.2, 3055.8 and 4074.4 W m^{-2} and incident laser power (P_0) levels of 1.0, 1.5 and 2.0 W, respectively. The thermal power (P) is proportional to incident laser power (P_0) through the absorptance (A) as $P = P_0A$. The cell was thermally insulated in a polystyrene foam coating to minimize the heat loss from the sample into the environment. The direction of thermal diffusion was along the direction of the B_0 field corresponding to the z direction.

The spatial and temporal variation of thermally induced nuclear spin phase shifts in the gel were measured in a coronal plane by a gradient echo (GRE) imaging sequence [24] using a 2 T NMR System (Bruker Biospin, USA). The imaging parameters were; bandwidth (BW) 16 kHz, echo time (T_E) 11 ms, repetition time (T_R) 90 ms, field of view (FOV) 64 mm, matrix size (M) 128 × 128, slice thickness (Δy) 4 mm, flip angle (θ) $\pi/4$, acquisition time (t_a) 23 s, number of excitations (NEX) 1 and the number of experiments (n) 30. The dimension of imaging volume was 10 mm × 4 mm × 50 mm in the cell.

The nuclear spin phase differences from voxels in the imaging slice were measured in space and time. The nuclear spin phase maps were constructed and unwrapped in two dimensional space (2D) using Flynn's minimum weighted discontinuity algorithm [25]. Using the symmetry, the measurements were reduced from 3D (xyz) to 2D (xz) and then to 1D (z) by successively averaging nuclear spin phase shifts in y-direction and xy-plane, respectively. Subsequently, the spatial and temporal variations of spin phase shifts were numerically fitted to the analytical heat conduction equation (Eq. (14)) using a least squares fitting algorithm, Levenberg–Marquardt Algorithm (LMA) [26,27], implemented in Matlab software (Mathworks, USA).

4. Results and discussion

The spatial and temporal variations of thermally induced nuclear spin phase shifts, following application of the constant power laser beam at $t = 0$ and $z = 0$, for a water-agarose gel are given in Figs. 2 and 3, respectively. Fig. 2 shows the nuclear spin phase

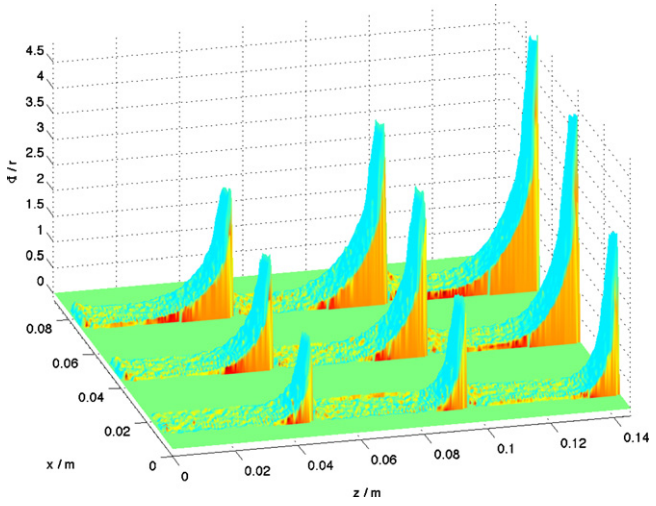

Fig. 2. Nuclear spin phase shift vs. space and time for three experiments corresponding to three power levels of 160, 240 and 320 mW (first, second and third rows) and three time points of 230, 460 and 690 s (left, middle and right columns), respectively.

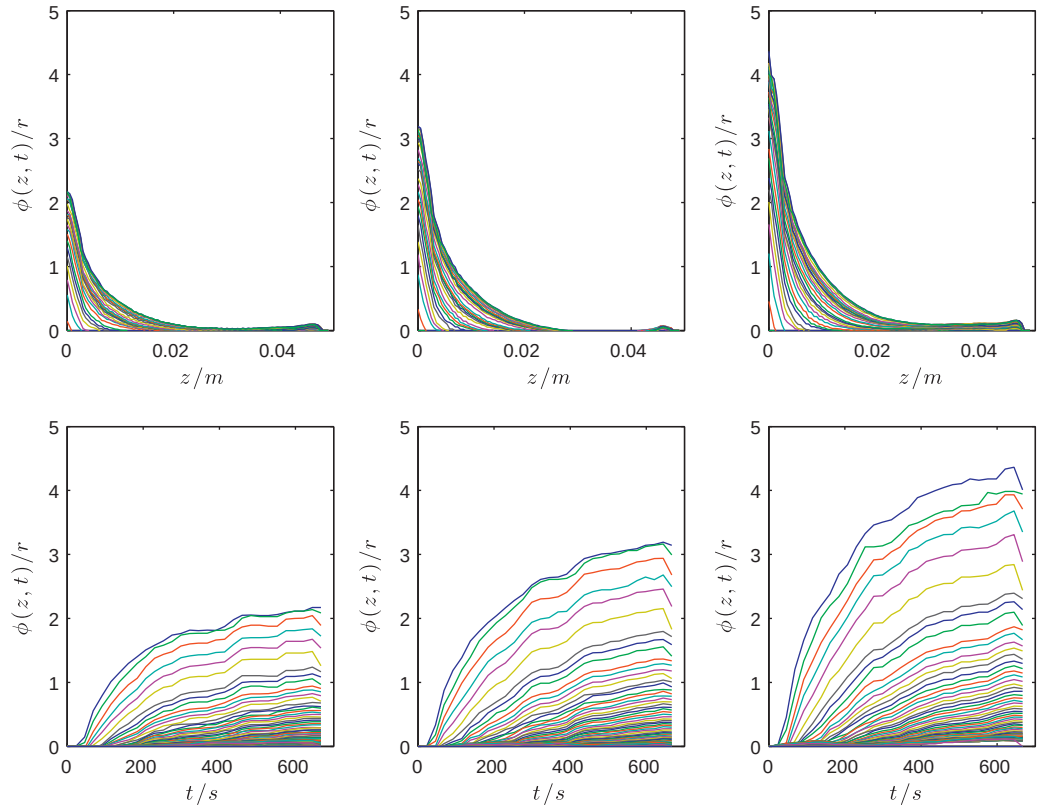

Fig. 3. Experimental nuclear spin phase shift vs. space (top row) and time (bottom row) at three power levels of 160, 240 and 320 mW (left, middle and right columns). Nuclear spin phase shift profiles gradually grow in space and time during heating. Absolute spin phase shift is shown here.

shift vs. space and time at high spatial resolution for three experiments corresponding to three different thermal power levels. The absolute magnitudes of the phase shifts for three time points and power levels are shown altogether in the *xz* plane for visualization.

Fig. 3 shows the phase shift spatially averaged in two dimensions (*xy* plane) and plotted vs. space (z) and time (t) for three power levels of 160, 240 and 320 mW.

The experimental plots of λ vs. $t^{1/2}$, ϕ_0 vs. λ and ϕ vs. t are shown in Fig. 4.

The slopes of lines in Fig. 4 correspond to $2\sqrt{\alpha}$, $f_0\phi_T/\kappa\sqrt{\pi}$ and $\dot{\phi}$ which yield, the thermal diffusivity (α), thermal conductivity (κ) and specific heat (c_p), respectively, in a single experiment. The diffusion length (λ) is independent of heat flux (f_0) but it is a function of thermal diffusion coefficient (α) and time (t) only whereas nuclear spin phase shift, both at the surface (ϕ_0) and spatially averaged (ϕ), is a function of heat flux (f_0) as shown in Fig. 4. Therefore, the thermal conductivity and specific heat can also be measured by fitting the data from multiple experiments corresponding to multiple power levels or heat flux levels.

The plots of average λ vs. $t^{1/2}$, S_0 vs. f_0 and $\dot{Q}$ vs. $\dot{\phi}$, yielding thermal diffusivity (α), thermal conductivity (κ) and specific heat (c_p), respectively, are shown in Fig. 5. The slopes of these lines correspond to $2\sqrt{\alpha}$, $\phi_T/\kappa\sqrt{\pi}$ and C_T/ϕ_T, respectively.

The results from three different transient experiments corresponding to three different power levels or flux levels and the results of fitting the data from three experiments at three flux levels are given in Table 1.

All three thermal parameters, thermal diffusivity, thermal conductivity and specific heat, can simultaneously be measured through a single experiment or multiple experiments as shown in Table 1.

Alternatively, for long times and short distances ($t \gg 0$ and $z \ll \lambda$), the limit of the transient solution will approach the steady state solution, and Fourier's heat conduction relation (Eq. (12)) from which the thermal conductivity can be measured directly by evaluating the nuclear spin phase shift gradients at each power levels.

Using the Eq. (9) and experimental NMR parameters of $T_E = 11$ ms, $\gamma = 2.674 \times 10^8\ \mathrm{r\,s^{-1}\,T^{-1}}$, $B_0 = 2\ \mathrm{T}$, $\sigma_T = -0.01\ \mathrm{ppm\,K^{-1}}$ and $\phi_T = -0.05885\ \mathrm{r\,K^{-1}}$, the temperature gradients and rates can be calculated through the nuclear spin phase shift gradients and rates as

$$\frac{\partial T}{\partial z} = \frac{1}{\phi_T}\frac{\partial \phi}{\partial z}, \quad \frac{\partial T}{\partial t} = \frac{1}{\phi_T}\frac{\partial \phi}{\partial t} \tag{21}$$

The variation of nuclear spin phase shifts corresponding to long times and short distances from the planar heat flux boundary for three flux levels is shown in Fig. 6.

For a known heat flux, by experimentally determining the temperature gradients, the thermal conductivity of the medium can be determined directly through Fourier's relation in a single experiment as shown in Table 2.

The heat flux levels of 2.0372, 3.0558 and 4.0744 mW/mm^2 in a plane perpendicular to the direction of magnetic field, B_0, in a 2 T magnet produced temperature gradients of −4.3, −6.0 and −7.8 K/mm along the direction of magnetic field (z).

The thermal conductivity of the 3% agarose–water gel was measured experimentally by two different methods, the transient method (Eq. (14)) and the steady state method (Eq. (12)), by evaluating the nuclear spin phase shift and its gradients near the planar heat flux boundary at three sequential experiments corresponding to three different heat flux levels as given in Tables 1 and 2, respectively. The results of fitting the data from all three experiments are given in the last columns of Tables 1 and 2.

The measurement of temperature gradients by NMR may be superior to any other invasive methods in substances with low thermal conductivity and shorter diffusion lengths over which the

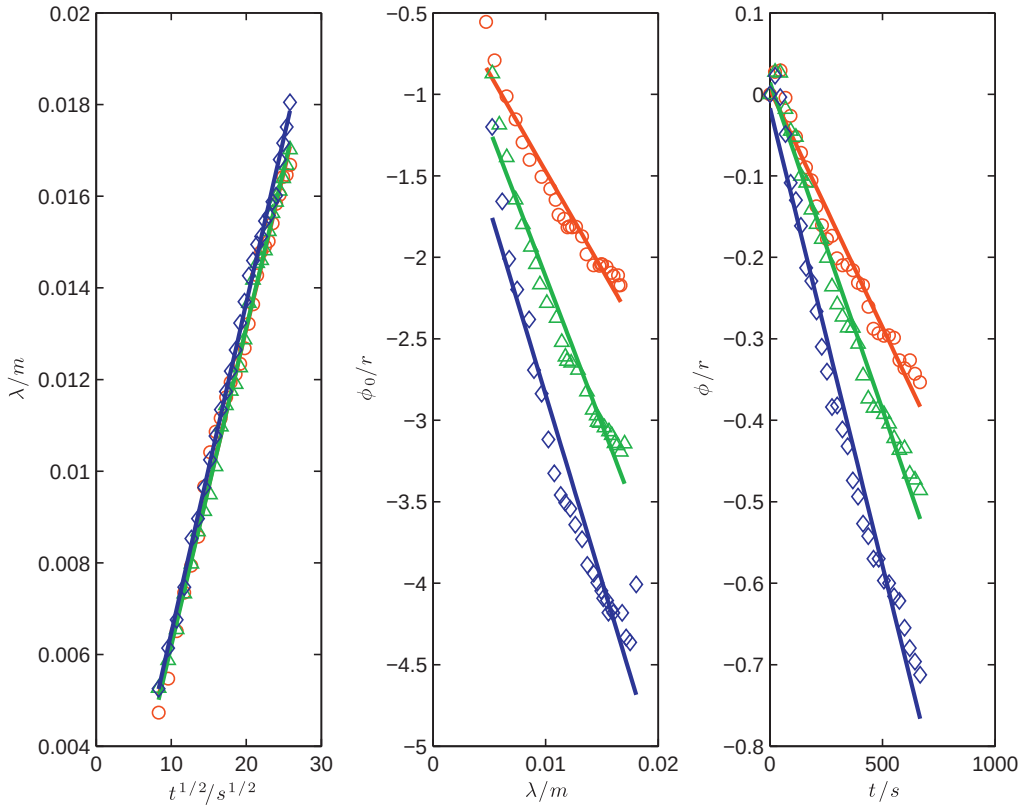

Fig. 4. Experimental plots of λ vs. $t^{1/2}$, ϕ_0 vs. λ and ϕ vs. t for three experiments corresponding to power levels of 160 mW (◯), 240 mW (△) and 320 mW (◊), respectively.

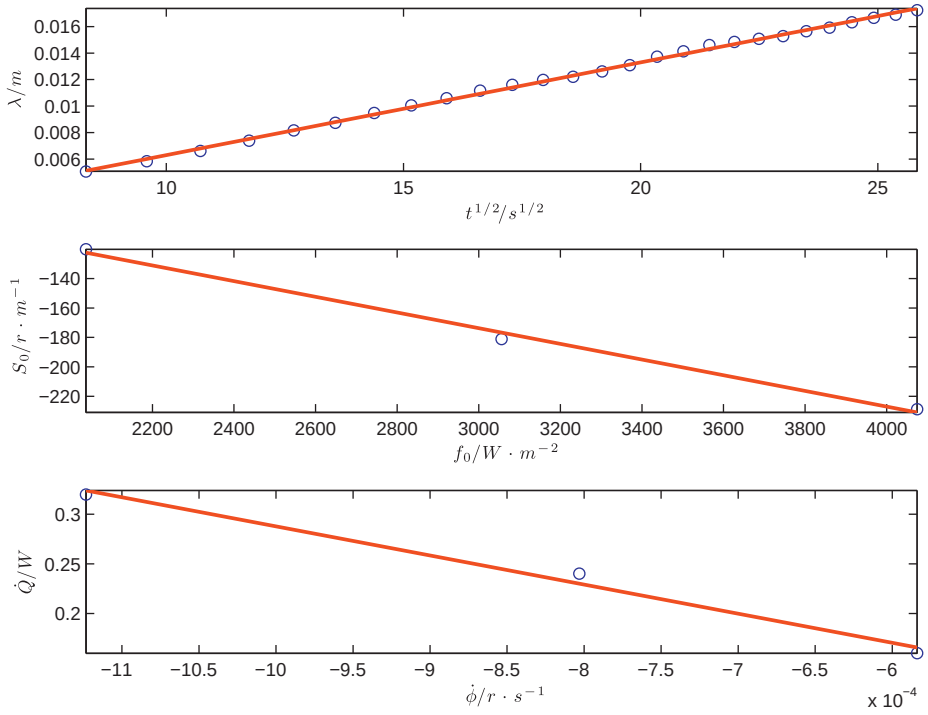

Fig. 5. Plots of λ vs. $t^{1/2}$ (top), S_0 vs. f_0 (middle) and $\dot{Q}$ vs. $\dot{\phi}$ (bottom) yielding thermal diffusivity (α), thermal conductivity (κ) and specific heat (c_p), respectively. The slopes of lines correspond to $2\sqrt{\alpha}$, $\phi_T/\kappa\sqrt{\pi}$ and C_T/ϕ_T, respectively.

Table 1
Experimental parameters and results of measurements of α, κ and c_p by three transient experiments at three heat flux levels for a 3% agarose–water gel.

Parameters	Experiment 1	Experiment 2	Experiment 3	Experiments 1–3
P_0 (W)	1.00	1.50	2.00	1.00–2.00
P (W)	0.16	0.24	0.32	0.16–0.32
f_0 (W m^{-2}) $\times 10^{-3}$	2.0372	3.0558	4.0744	2.0372–4.0744
α (m^2 s^{-1}) $\times 10^7$	1.1705 ± 0.0166	1.2028 ± 0.0134	1.2962 ± 0.0146	1.2226 ± 0.0100
κ (W m^{-1} K^{-1})	0.5633 ± 0.0255	0.5603 ± 0.0235	0.5914 ± 0.0335	0.6225 ± 0.0443
c_p (J kg^{-1} K^{-1}) $\times 10^{-3}$	4.1903 ± 0.1509	4.5699 ± 0.1228	4.3561 ± 0.1312	4.4831 ± 0.4849
$\kappa/\rho c_p$ (m^2 s^{-1}) $\times 10^7$	1.3443 ± 0.0125	1.2260 ± 0.0185	1.3578 ± 0.0360	1.3887 ± 0.0520

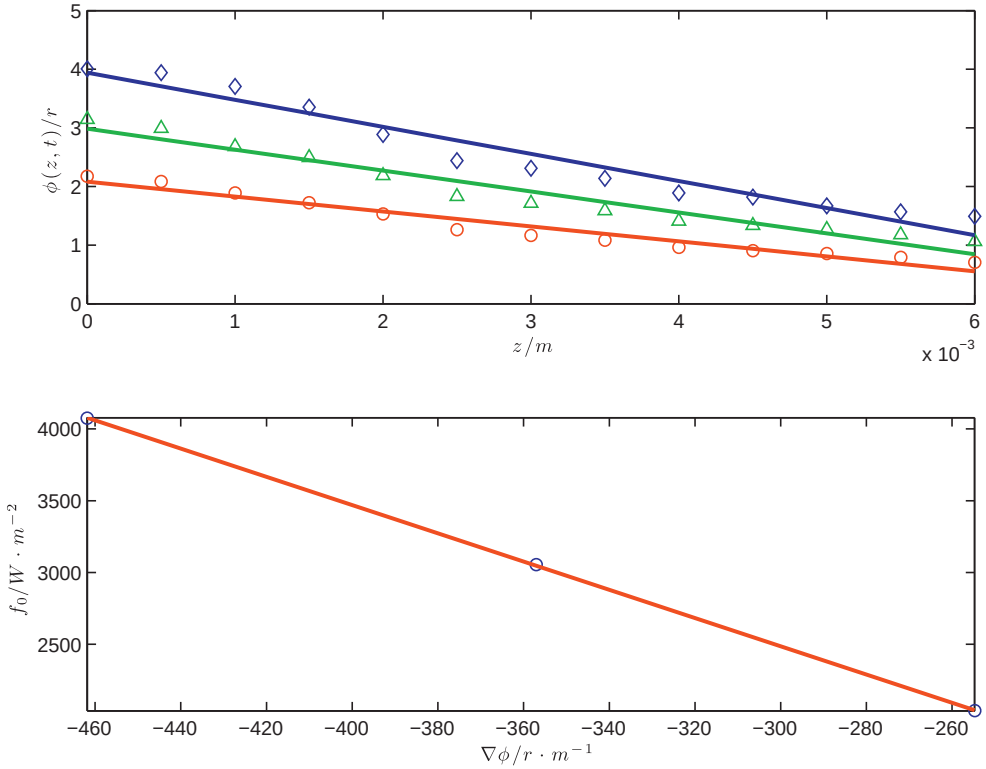

Fig. 6. Experimental $\phi(z, t)$ vs. z over a distance of 6 mm from the planar heat flux boundary (top) and experimental f_0 vs. $\nabla\phi$ (bottom) for three experiments at three heat flux levels.

Table 2
Nuclear spin phase shift gradients, temperature gradients and the thermal conductivity measured by three steady state experiments at three different heat flux levels for a 3% agarose–water gel.

Parameters	Experiment 1	Experiment 2	Experiment 3	Experiments 1–3
f_0 (W m^{-2}) $\times 10^{-3}$	2.0372	3.0558	4.0744	2.0372 to 4.0744
$\nabla\phi$ (r m^{-1}) $\times 10^{-3}$	−0.2547 ± 0.0170	−0.3570 ± 0.0245	−0.4618 ± 0.0324	−0.2547 to −0.4618
∇T (K m^{-1}) $\times 10^{-3}$	−4.3286 ± 0.2905	−6.0674 ± 0.6173	−7.8478 ± 0.5517	−4.3286 to −7.8478
κ (W m^{-1} K^{-1})	0.4706 ± 0.0316	0.5036 ± 0.0346	0.5192 ± 0.0365	0.5789 ± 0.0040

temperature gradients are formed and which must be measured by a non-invasive and non-contact method. The thermal properties of 3% agarose–water gel measured by NMR method here are close to the thermal properties of water in the literature.

The agreement between the theory and the experiment was very high with mean r-square of fitting of 0.988, 0.989 and 0.988 for experiments 1, 2 and 3, respectively. The standard errors of the measurements for each of the three thermal parameters were similar for the three experiments. The percent errors (%) for the experiments 1, 2 and 3 were 1.41, 1.11 and 1.12 for thermal diffusivity; 4.52, 4.19 and 5.66 for thermal conductivity; and 3.60, 2.68 and 3.01 for specific heat, respectively. The measurement of thermal diffusivity is independent of the magnitude of the heat flux whereas the measurements of thermal conductivity and specific heat are not. The standard errors for the results of the linear regression of the data from three experiments were 0.82, 7.12 and 10.82% for thermal diffusivity, thermal conductivity and specific heat, respectively. The variation in the mean values of the thermal parameters may be due to the variations in the laser power, laser beam profile, beam alignment, absorption or heat loss between the experiments.

5. Conclusion

Fourier's heat conduction relation has been experimentally evaluated using NMR imaging. Appropriate analyses of the spatial and temporal variations of changes in proton resonance frequency yield three thermal properties; thermal diffusivity, thermal conductivity and specific heat, simultaneously in a single experiment. This is made possible because of the relatively high spatial and tem-

poral resolutions achievable with NMR imaging. This NMR method can effectively be applied to the measurement of thermal properties of a wide range of materials.

References

[1] B. Wunderlich, Temperature-modulated calorimetry in the 21st century, Thermochim. Acta 355 (July (43)) (2000).
[2] B. Wunderlich, The tribulations and successes on the road from DSC to TMDSC in the 20th century the prospects for the 21st century, J. Therm. Anal. Calorim. 78 (2004) 7.
[3] W.A. Wakeham, et al., Thermophysical property measurements: the journey from accuracy to fitness for purpose, Int. J. Thermophys. 28 (April (372)) (2007).
[4] E.S. Watson, J. Justin, N. Brenner, M.J. Oneill, Differential scanning calorimeter for quantitative differential thermal analysis, Anal. Chem. 36 (1964) 1233.
[5] P.S. Gill, S.R. Sauerbrunn, M. Reading, Modulated differential scanning calorimetry, J. Therm. Anal. 40 (1993) 931.
[6] M. Reading, A. Luget, R. Wilson, Modulated differential scanning calorimetry, Thermochim. Acta 238 (June (295)) (1994).
[7] W.J. Parker, R.J. Jenkins, G.L. Abbott, C.P. Butler, Flash method of determining thermal diffusivity heat capacity, and thermal conductivity, J. Appl. Phys. 32 (1961) 1679.
[8] M.J. Assael, K.D. Antoniadis, W.A. Wakeham, Historical evolution of the transient hot-wire technique, Int. J. Thermophys. 31 (June) (2010) 1051.
[9] W. Wakeham, M. Assael, The Measurement Instrumentation and Sensors Handbook on CD-ROM, CRC Press, 1999.
[10] S.E. Gustafsson, E. Karawacki, M.N. Khan, Transient hot-strip method for simultaneously measuring thermal-conductivity and thermal-diffusivity of solids and fluids, J. Phys. D: Appl. Phys. 12 (1979) 1411.
[11] D.H. Gultekin, Thesis (Ph.D.), Yale University, 2002.
[12] D.H. Gultekin, J.C. Gore, 9th International Congress on Hyperthermic Oncology, St. Louis, Missouri, USA, 2004, p. 140.
[13] D.H. Gultekin, J.C. Gore, Submitted to 9th International Society for Magnetic Resonance in Medicine, November 14, 2000.
[14] D.H. Gultekin, J.C. Gore, International Society for Magnetic Resonance in Medicine, Kyoto, Japan, 2004.
[15] D.H. Gultekin, J.C. Gore, Measurement of thermal diffusivity by magnetic resonance imaging, Magn. Reson. Imaging 24 (2006) 1203.
[16] D.H. Gultekin, J.C. Gore, 9th International Congress on Hyperthermic Oncology, St. Louis, Missouri, USA, 2004, p. 141.
[17] D.H. Gultekin, J.C. Gore, Measurement of specific heat and specific absorption rate by nuclear magnetic resonance, Thermochim. Acta 503 (May (100)) (2010).
[18] H.S. Carslaw, J.C. Jaeger, Conduction of Heat in Solids, 2nd ed., Clarendon Press/Oxford University Press, Oxford, Oxfordshire/New York, 1986, p. viii, 510 p.
[19] J. Fourier, The Analytical Theory of Heat, Cambridge University Press, London, 1878, p. 466.
[20] W.E. Lamb, Internal diamagnetic fields, Phys. Rev. 60 (1941) 817.
[21] N.F. Ramsey, Magnetic shielding of nuclei in molecules, Phys. Rev. 78 (1950) 699.
[22] J.C. Hindman, Proton resonance shift of water in gas and liquid states, J. Chem. Phys. 44 (1966) 4582.
[23] G.M. Hale, M.R. Querry, Optical-constants of water in 200 nm to 200 μm wavelength region, Appl. Opt. 12 (1973) 555.
[24] A. Haase, J. Frahm, D. Matthaei, W. Hanicke, K.D. Merboldt, Flash imaging. Rapid NMR imaging using low flip-angle pulses, J. Magn. Reson. 67 (April (258)) (1986).
[25] T.J. Flynn, Two-dimensional phase unwrapping with minimum weighted discontinuity, J. Opt. Soc. Am. A 14 (1997) 2692.
[26] K. Levenberg, A method for the solution of certain non-linear problems in least squares, Q. Appl. Math. 2 (1944) 164.
[27] D. Marquardt, An algorithm for least-squares estimation of nonlinear parameters, SIAM J. Appl. Math. 11 (1963) 431.